Investigation on the Doppler shifts induced by 1-D ocean surface wave displacements by the first order small slope approximation theory: comparison of hydrodynamic models*

Wang Yun-Hua(王运华)[a], Zhang Yan-Min(张彦敏)[b]†, and Guo Li-Xin(郭立新)[c]

[a] *Ocean Remote Sensing Institute, Ocean University of China, Qingdao* 266003, *China*
[b] *Department of Physics, Ocean University of China, Qingdao* 266100, *China*
[c] *School of Science, Xidian University, Xi'an* 710071, *China*

(Received 6 November 2009; revised manuscript received 8 December 2009)

Based on the first order small slope approximation theory (SSA-I) for oceanic surface electromagnetic scattering, this paper predicts the Doppler shifts induced by wave displacements. Theoretical results from three distinct hydrodynamic models are compared: a linear model, the nonlinear Barrick model, and the nonlinear Creamer model. Meanwhile, the predicted Doppler shifts are also compared with the results associated to the resonant Bragg waves and the so-called long waves in the framework of the two-scale model. The dependences of the predicted Doppler shifts on the incident angle, the radar frequency, and the wind speed are discussed. At large incident angles, the predicted Doppler shifts for the linear and nonlinear Barrick models are found to be insensitive to the wind speed and this phenomenon is not coincident with the experimental data. The conclusions obtained in this paper are promising for better understanding the properties of time dependent radar echoes from oceanic surfaces.

Keywords: Doppler shifts, sea surface model, SSA-I, electromagnetic scattering
PACC: 4120, 4110H

1. Introduction

As an important parameter of the Doppler spectrum, Doppler shift corresponds to a power-weighted mean line-of-sight velocity of scatters. Thus, the investigations[1−6] on Doppler shifts of electromagnetic echoes from time-varying oceanic surfaces are of practical importance in a number of research areas such as sea surface wind retrieving, sea waves monitoring, and oceanic surface current measuring. In Refs. [7] and [8], for moderate- and low-grazing angles, the Doppler spectra calculations based on the composite sea surface model(the two-scale model (TSM)) and the comparisons with experimental data were reported. Unfortunately, if the incident angle is smaller than 20°, the Doppler spectra model given by TSM is insufficient because the Bragg-scattering mechanism is invalid. In Ref. [9], Doppler shifts of backscattered fields from sea surfaces were predicted by asymptotic electromagnetic wave scattering theories (including Kirchhoff, the first order small slope and the Local curvature approximations). As is pointed out in Ref. [9], the predicted Doppler shifts for the Kirchhoff and the first order small slope approximations (SSA-I) in co-polarised configuration are independent on the polarisation state. On the other hand, the local curvature solutions yield significant differences between co-polarised predicated Doppler shifts. However, it should be mentioned that only the linear sea surface model has been considered in Ref. [9]. It is now well established that the wave–wave interactions between harmonic waves cannot be neglected if one aims at interpreting the Doppler spectra of backscattered fields.[10−12] In our simulations, two one dimensional (1-D) nonlinear sea surface models are also included. One is the nonlinear surface model proposed by Barrick and Weber in Ref. [13]. In this model, a general hydrodynamic solution is derived for arbitrary gravity-wave fields on sea surface by the perturbation techniques and sea surface spectrum up to second order is obtained. The other nonlinear sea surface model was reported in Ref. [14] by Creamer *et al.* In this model, the Hamiltonian formalism under the

*Project supported by the Young Scientists Fund of the National Natural Science Foundation of China (Grant No. 40906088) and Specialized Research Fund for the Doctoral Program of Higher Education of China.
†Corresponding author. E-mail: zhangyanmin79@163.com
© 2010 Chinese Physical Society and IOP Publishing Ltd

weak wave-turbulence theory is utilized to simulate the interactions between harmonic waves.

In this paper, Doppler shifts induced by ocean surface wave displacements are predicted by an asymptotic electromagnetic method based on SSA-I[15] for various radar frequencies and wind speeds. And the numerical results are compared for three distinct hydrodynamic models. This paper is organized as follows. In Section 2, the outlines of SSA-I are described. The three hydrodynamic models used in this paper are described in Section 3. Section 4 presents the asymptotic solutions to define Doppler frequency. While Section 5 is devoted to the results and comments. Final conclusions are presented in Section 6.

2. The scattering model

In this paper, the sea surface elevation is represented by $z = z(x,t)$, where x denotes the position in x-axis and t is the time dependence of the sea surface.

Suppose a plane wave is incident on the sea surface and given by

$$E^{\rm in} = \exp[{\rm j}k(x\sin\theta_{\rm i} - z\cos\theta_{\rm i})], \tag{1}$$

where k is the wave number of the incident field, and $\theta_{\rm i}$ denotes the incident angle.

The scattering amplitude (SA)$S_{\alpha\alpha}(\boldsymbol{k},\boldsymbol{k}_0)$ in the framework of the SSA-I can be expressed as[15]

$$\begin{aligned} S_{\alpha\alpha}k_{\rm sx},k_{\rm ix},t) \;=\; & 2\frac{(k_{\rm sz}k_{\rm iz})^{1/2}}{k_{\rm sz}+k_{\rm iz}}B_{\alpha\alpha}(k_{\rm sx},k_{\rm ix}) \\ & \times\int\frac{{\rm d}x}{2\pi}\exp[{\rm j}(k_{\rm ix}-k_{\rm sx})x \\ & +{\rm j}(k_{\rm sz}+k_{\rm iz})z(x,t)], \end{aligned} \tag{2}$$

with

$$k_{ix} = k\sin\theta_{\rm i}, \tag{2a}$$

$$k_{sx} = k\sin\theta_s, \tag{2b}$$

$$k_{\rm iz} = k\cos\theta_{\rm i}, \tag{2c}$$

$$k_{\rm sz} = k\cos\theta_s, \tag{2d}$$

$$B_{\alpha\alpha}(k_{\rm sx},k_{\rm ix}) = \begin{cases} -\dfrac{\varepsilon-1}{(q^{(1)}+q^{(2)})(q_0^{(1)}+q_0^{(2)})}\dfrac{\omega^2}{c^2}\dfrac{\boldsymbol{k}\cdot\boldsymbol{k}_0}{kk_0} & \alpha\alpha_0 = {\rm HH}, \\ \dfrac{\varepsilon-1}{(\varepsilon q^{(1)}+q^{(2)})(\varepsilon q_0^{(1)}+q_0^{(2)})}\left(q^{(2)}q_0^{(2)}\dfrac{\boldsymbol{k}\cdot\boldsymbol{k}_0}{kk_0}-\varepsilon kk_0\right), & \alpha\alpha_0 = {\rm VV}, \end{cases} \tag{2e}$$

$$q_0^{(1)} = \sqrt{\frac{\omega^2}{c^2}-k_0^2}, \quad q_0^{(2)} = \sqrt{\varepsilon\frac{\omega^2}{c^2}-k_0^2}, \quad \mathrm{Im}\, q_0^{(1,2)} \geq 0, \tag{2f}$$

$$q^{(1)} = \sqrt{\frac{\omega^2}{c^2}-k^2}, \quad q^{(2)} = \sqrt{\varepsilon\frac{\omega^2}{c^2}-k^2}, \quad \mathrm{Im}\, q^{(1,2)} \geq 0, \tag{2g}$$

where the subscript α represents H (horizontal) or V(vertical) polarisation, ε is a general complex dielectric constant of sea water, ω is the anglular frequency of the incident field and c denotes the velocity of light.

The expression for a scattering cross section is directly related to the second-order statistical moment of the SA, and the statistical evaluation mostly concerns

$$\begin{aligned} \langle S(k_{\rm sx},k_{\rm ix},t+\Delta t)S^*(k_{\rm sx},k_{\rm ix},t)\rangle \;=\; & \left\{\frac{(k_{\rm sz}k_{\rm iz})^{1/2}B(k_{\rm sx},k_{\rm ix})}{\sqrt{2}\pi(k_{\rm sz}+k_{\rm iz})}\right\}^2\int\exp[{\rm j}(k_{\rm ix}-k_{\rm sx})\Delta x]\langle\exp\{{\rm j}(k_{\rm sz}+k_{\rm iz}) \\ & \times[z(x',t+\Delta t)-z^*(x,t)]\}\rangle{\rm d}x'{\rm d}x \end{aligned} \tag{3}$$

where $x' = x+\Delta x$, the superscript $*$ in z^* represents the conjugate of z.

Equation (3) contains ensemble average $\langle\exp[{\rm j}(k_{\rm sz}+k_{\rm iz})(z-z^*)]\rangle$. Utilizing the method of characteristic function in Ref. [16], we can find the ensemble average up to the third power in $(k_{\rm sz}+k_{\rm iz})$ as

$$\langle\exp[{\rm j}(k_{\rm sz}+k_{\rm iz})(z-z^*)]\rangle \approx \exp[(k_{\rm sz}+k_{\rm iz})^2(\rho-\sigma^2) - {\rm j}\frac{(k_{\rm sz}+k_{\rm iz})^3}{3}\sigma^3 S_{12}], \tag{4}$$

with

$$\rho(\Delta x,\Delta t) = \langle z(x+\Delta x,t+\Delta t)z(x,t)\rangle\,, \tag{5}$$

$$S_{12} = \frac{\langle z^2(x+\Delta x,t+\Delta t)z(x,t)\rangle - \langle z(x+\Delta x,t+\Delta t)z^2(x,t)\rangle}{\sigma^3}, \tag{6}$$

where σ^2 and ρ denote the variance and correlation function of the sea surface roughness, respectively.

For the Barrick and the Creamer hydrodynamic models, $z(x,t)$ is a nonlinear variable. The geometrical structures of the sea surface elevations simulated by these two models are similar to the Stokes waves in many important respects, such as vertical skewness of sea waves. However, both models do not show any asymmetry due to tilted crests in the horizontal direction, which is referred to as horizontal skewness. Just as pointed out in Ref. [17], S_{12} equals zero if a random surface profile can not reflect the horizontal skewness. Therefore, the characteristic functions $\langle \exp[\mathrm{j}(k_{\mathrm{s}z}+k_{\mathrm{i}z})(z-z^*)]\rangle$ for the Barrick and Creamer models can be simplified as

$$\begin{aligned}&\langle \exp[\mathrm{j}(k_{\mathrm{s}z}+k_{\mathrm{i}z})(z-z^*)]\rangle\\ &\approx \exp[(k_{\mathrm{s}z}+k_{\mathrm{i}z})^2(\rho-\sigma^2)].\end{aligned} \tag{7}$$

Substituting Eq. (7) into Eq. (3) and using the relation between normalized radar cross-section (NRCS) $\sigma_{\alpha\alpha}$ and the scattering amplitude $S_{\alpha\alpha}(k_{\mathrm{s}x},k_{\mathrm{i}x})$, we obtain the expression for a dimensionless scattering cross section as

$$\begin{aligned}\sigma_{\alpha\alpha}(k_{\mathrm{s}x},k_{\mathrm{i}x},t) =\ & \frac{1}{\pi}\left|\frac{2k_{\mathrm{i}z}k_{\mathrm{s}z}B_{\alpha\alpha}(k_{\mathrm{s}x},k_{\mathrm{i}x})}{k_{\mathrm{i}z}+k_{\mathrm{s}z}}\right|^2\\ &\times \exp[-(k_{\mathrm{i}z}+k_{\mathrm{s}z})^2\sigma^2]\\ &\times \int \{\exp[(k_{\mathrm{i}z}+k_{\mathrm{s}z})^2\rho(x,t)]-1\}\\ &\times \exp[\mathrm{j}(k_{\mathrm{i}z}-k_{\mathrm{s}z})x]\mathrm{d}x.\end{aligned} \tag{8}$$

For simplifying the notations, in the correlation function expressions, Δx and Δt have been replaced by x and t respectively. And the correlation function $\rho(x,t)$ for sea surface roughness can also be written as

$$\rho(x,t)=\int W_t(K,t)\exp[\mathrm{j}(Kx)]\mathrm{d}K, \tag{9}$$

where $W_t(K,t)$ denotes the sea surface spectrum at a given time t.

3. Sea surface spectrum at a given time t

In order to evaluate the correlation function $\rho(x,t)$, in general, it is convenient to obtain the surface temporal spectrum $W_t(K,t)$ first.

3.1. Surface temporal spectrum for linear surface

The correlation function of a linear sea surface is defined as[18]

$$\rho_{\mathrm{L}}(x,t)=\int_{-\infty}^{+\infty}\int_{-\infty}^{+\infty} W(K,\omega)\exp[\mathrm{j}(Kx-\omega t)]\mathrm{d}\omega\mathrm{d}K, \tag{10}$$

where K and ω denote the spatial wave number and the angular frequency of a harmonic wave, respectively. And $W(K,\omega)$ is

$$W(K,\omega)=\frac{1}{2}\varphi(K)\delta(\omega-\sqrt{gK})+\frac{1}{2}\varphi(-K)\delta(\omega+\sqrt{gK}),\quad K\geq 0, \tag{11}$$

here g denotes the gravity acceleration constant, $\delta(\bullet)$ is the Dirac-delta function and $\varphi(K)$ is the omni-directional sea surface spectrum.[19]

Substituting Eq. (11) into Eq. (10), we obtain

$$\begin{aligned}\rho_{\mathrm{L}}(x,t) =\ & \frac{1}{2}\int_{-\infty}^{+\infty}\int_{-\infty}^{+\infty}[\varphi(K)\delta(\omega-\sqrt{g\,|K|})+\varphi(-K)\delta(\omega+\sqrt{g\,|K|})]\exp[\mathrm{j}(Kx-\omega t)]\mathrm{d}\omega\mathrm{d}K\\ =\ & \frac{1}{2}\int_{-\infty}^{0}\varphi(K)\exp[\mathrm{j}(Kx+\sqrt{g\,|K|}t)]\mathrm{d}K+\frac{1}{2}\int_{0}^{+\infty}\varphi(K)\exp[\mathrm{j}(Kx-\sqrt{g\,|K|}t)]\mathrm{d}K\\ =\ & \int_{-\infty}^{+\infty}W_t(K,t)\exp(\mathrm{j}Kx)\mathrm{d}K,\end{aligned} \tag{12}$$

where the sea surface temporal spectrum can be written as

$$W_t(K,t)=\begin{cases}\dfrac{1}{2}\varphi(K)\exp(-\mathrm{j}\sqrt{gK}t), & K\geq 0,\\ \dfrac{1}{2}\varphi(K)\exp(\mathrm{j}\sqrt{g\,|K|}t), & K<0.\end{cases} \tag{13}$$

3.2. Surface temporal spectrum for nonlinear Barrick surface

In Ref. [13], the sea surface temporal spectrum up to second-order were obtained by Barrick and Weber, utilizing the Stokes perturbation technique. The second-order spectrum is expressed as

$$W_B(\boldsymbol{K},\omega) = W(\boldsymbol{K},\omega) + W_2(\boldsymbol{K},\omega), \tag{14}$$

where $W(\boldsymbol{K},\omega)$ denotes the sea surface spectrum corresponding a linear sea surface. And $W_2(\boldsymbol{K},\omega)$ denotes the second-order spectrum, which is

$$W_2(\boldsymbol{K},\omega) = -\sum_{m,m'=\pm 1}\int_{-\infty}^{+\infty}\int_{-\infty}^{+\infty} A^2\varphi(m\boldsymbol{\kappa})\varphi(m'\boldsymbol{\kappa}')\delta(\omega - m\sqrt{g\,|\boldsymbol{\kappa}|} - m'\sqrt{g\,|\boldsymbol{\kappa}'|})\mathrm{d}\boldsymbol{p}, \tag{15}$$

here $\boldsymbol{\kappa} = 0.5\boldsymbol{K} + \boldsymbol{p}$, $\boldsymbol{\kappa}' = 0.5\boldsymbol{K} - \boldsymbol{p}$. And the quantity A is defined by[20]

$$A = \begin{cases} \dfrac{1}{2}\left[|\boldsymbol{\kappa}| + |\boldsymbol{\kappa}'| + \dfrac{\omega_0\omega_0'(1-\hat{\kappa}\hat{\kappa}')}{g}\left(\dfrac{g\,|\boldsymbol{K}| + \omega^2}{g\,|\boldsymbol{K}| - \omega^2}\right)\right], \\ 0 \quad \text{if} \quad \boldsymbol{\kappa} = -\boldsymbol{\kappa}' \quad \text{and} \quad \omega_0 = \omega_0', \end{cases} \tag{16}$$

with $\omega_0 = \sqrt{g\,|\boldsymbol{\kappa}|}$, $\omega_0' = \sqrt{g\,|\boldsymbol{\kappa}'|}$.

In Eq. (15), the vector wave numbers are replaced by scalar wave numbers for 1-D waves, so the double integral becomes a single integral. This permits us to evaluate the integral because of the Dirac-delta function. After a straightforward manipulation, we can obtain the expression for the sea surface temporal spectrum as

$$W_{Bt}(K,t) = W_t(K,t) + \frac{1}{2}K^2\int_{-\infty}^{+\infty} W_t(q,t)\cdot W_t(K-q,t)\mathrm{d}q. \tag{17}$$

It shows that Eq. (17) has N^2 numerical constants due to the integration. However, we can find that the integral is a convolution for $W_t(K,t)$. Then, using the properties of Fourier transform, we can rewrite Eq. (17) as following

$$W_{Bt}(K,t) = W_t(K,t) + \frac{1}{2}K^2\int_{-\infty}^{+\infty} \rho_{\mathrm{L}}^2(x,t)\exp(-\mathrm{j}Kx)\mathrm{d}x. \tag{18}$$

Equation (18) can be computed by fast Fourier transform with $N\log N$ constants.

3.3. Surface temporal spectrum for nonlinear Creamer surface

In Ref. [14], Creamer *et al.* derived a nonlinear sea surface model for gravity waves. In this model, the way to simulate nonlinear effect is the Hamiltonian formalism under the weak wave-turbulence theory. Formulation of such a 1D surface is

$$z_C(x,t) = \int \hat{z}_C(K)\exp[\mathrm{j}(Kx - \omega t)]\mathrm{d}K \tag{19}$$

with

$$\hat{z}_C(K) = \frac{1}{|K|}\int_{-\infty}^{+\infty}\{\exp[\mathrm{j}Kz_{\mathrm{L}}(x,t)] - 1\} \times \exp(-\mathrm{j}Kx)\mathrm{d}x, \tag{20}$$

where $z_{\mathrm{L}}(x,t)$ denotes the linear surface elevation.

Using Eqs. (12) and (19), we can obtain

$$W_{Ct}(K,t)\delta(K+P) = \frac{1}{2\pi}\left\langle \hat{z}_C(K)\hat{z}_C(P)\right\rangle, \tag{21}$$

where $\langle\bullet\rangle$ denotes ensemble average.

Substituting Eq. (20) into Eq. (21), after a lengthy but straightforward manipulation, we obtain the sea temporal spectrum for the nonlinear Creamer surface model as

$$W_{Ct}(K,t) = \frac{1}{2}K^2\int_{-\infty}^{+\infty}\exp(-\mathrm{j}Kx)\exp[-K^2\rho_{\mathrm{L}}(0,0)] \times\{\exp[K^2\rho_{\mathrm{L}}(x,t)] - 1\}\mathrm{d}x \tag{22}$$

4. Doppler shift

To express the correlation function as a function of the time from a given state, we will consider only very short time lags, i.e. $t << 1.0$s. Thus, we can perform a Taylor expansion around zero at first order to describe the changes of the correlation function for sea surface roughness during this small time lag, i.e.

$$\rho(x,t) \approx \rho(x,0) + t\left.\frac{\partial\rho(x,t)}{\partial t}\right|_{t=0} + \ldots. \tag{23}$$

Using Eq. (8) and (23), we can rewrite the scattering cross section $\sigma_{\alpha\alpha}(k_{\mathrm{s}x}, k_{\mathrm{i}x}, t)$ as

$$\sigma_{\alpha\alpha}(t) \approx \sigma^0_{\alpha\alpha}(0) + \sigma^1_{\alpha\alpha}(t), \tag{24}$$

where

$$\begin{aligned}\sigma^0_{\alpha\alpha}(0) &= \frac{1}{\pi}\left|\frac{2k_{\mathrm{i}z}k_{\mathrm{s}z}B_{\alpha\alpha}(k_{\mathrm{s}x}, k_{\mathrm{i}x})}{k_{\mathrm{i}z}+k_{\mathrm{s}z}}\right|^2 \exp[-(k_{\mathrm{i}z}+k_{\mathrm{s}z})^2\sigma^2] \\ &\quad\times\int\{\exp[(k_{\mathrm{i}z}+k_{\mathrm{s}z})^2\rho(x,0)]-1\}\exp[\mathrm{j}(k_{\mathrm{i}z}-k_{\mathrm{s}z})x]\mathrm{d}x, \qquad (25)\\ \sigma^1_{\alpha\alpha}(t) &= t\times\sigma'^1_{\alpha\alpha}(0) = t\times\frac{1}{\pi}\left|2k_{\mathrm{i}z}k_{\mathrm{s}z}B_{\alpha\alpha}(k_{\mathrm{s}x}, k_{\mathrm{i}x})\right|^2\exp[-(k_{\mathrm{i}z}+k_{\mathrm{s}z})^2\sigma^2] \\ &\quad\times\int\rho'(x,0)\exp[(k_{\mathrm{i}z}+k_{\mathrm{s}z})^2\rho(x,0)]\exp[\mathrm{j}(k_{\mathrm{i}z}-k_{\mathrm{s}z})x]\mathrm{d}x, \qquad (26)\end{aligned}$$

with

$$\rho'(x,0) = \left.\frac{\partial\rho(x,\mathrm{t})}{\partial t}\right|_{t=0}. \tag{27}$$

Under the condition of small time lag, i.e. $t \ll 1.0$ s, we have

$$\begin{aligned}\sigma_{\alpha\alpha}(t) &= \sigma^0_{\alpha\alpha}(0)\left[1+\frac{t\times\sigma'^1_{\alpha\alpha}(t)}{\sigma^0_{\alpha\alpha}(0)}\right] \\ &= \sigma^0_{\alpha\alpha}(0)\left\{1+\frac{t\times\left[\sigma'^1_{\alpha\alpha\,r}(0)+\mathrm{j}\sigma'^1_{\alpha\alpha\,i}(0)\right]\left[\sigma^0_{\alpha\alpha\,r}(0)-\mathrm{j}\sigma^0_{\alpha\alpha\,i}(0)\right]}{\left[\sigma^0_{\alpha\alpha\,r}(0)+\mathrm{j}\sigma^0_{\alpha\alpha\,i}(0)\right]\left[\sigma^0_{\alpha\alpha\,r}(0)-\mathrm{j}\sigma^0_{\alpha\alpha\,i}(0)\right]}\right\} \\ &= \sigma^0_{\alpha\alpha}(0)\left[1+\frac{t\times\sigma'^1_{\alpha\alpha\,r}(0)\sigma^0_{\alpha\alpha\,r}(0)+t\times\sigma'^1_{\alpha\alpha\,i}(0)\sigma^0_{\alpha\alpha\,i}(0)}{\left|\sigma^0_{\alpha\alpha}(0)\right|^2}+\mathrm{j}\frac{\sigma'^1_{\alpha\alpha\,i}(0)\sigma^0_{\alpha\alpha\,r}(0)-\sigma'^1_{\alpha\alpha\,r}(0)\sigma^0_{\alpha\alpha\,i}(0)}{\left|\sigma^0_{\alpha\alpha}(0)\right|^2}\times t\right] \\ &\approx \sigma^0_{\alpha\alpha}(0)\exp\left[\mathrm{j}\frac{\sigma'^1_{\alpha\alpha\,i}(0)\sigma^0_{\alpha\alpha\,r}(0)-\sigma'^1_{\alpha\alpha\,r}(0)\sigma^0_{\alpha\alpha\,i}(0)}{\left|\sigma^0_{\alpha\alpha}(0)\right|^2}\times t\right], \qquad (28)\end{aligned}$$

where $\sigma^0_{\alpha\alpha\,r}(0)$, $\sigma^0_{\alpha\alpha\,i}(0)$ and $\sigma'^1_{\alpha\alpha\,r}(0)$, $\sigma'^1_{\alpha\alpha\,i}(0)$ denote the real and the imaginary part of $\sigma^0_{\alpha\alpha}(t)$ and $\sigma'^1_{\alpha\alpha}(t)$, respectively.

Introducing the Fourier transform of the NRCS

$$\sigma_{\alpha\alpha}(f_{\mathrm{D}}) = \int\sigma_{\alpha\alpha}(t)\exp(-\mathrm{j}2\pi f_{\mathrm{D}}t)\mathrm{d}t, \tag{29}$$

we can get the Doppler spectrum of the backscattered field as

$$\begin{aligned}\sigma_{\alpha\alpha}(f_{\mathrm{D}}) &= \int\sigma^0_{\alpha\alpha}(0)\exp\left[\mathrm{j}\frac{\sigma'^1_{\alpha\alpha\,i}(0)\sigma^0_{\alpha\alpha\,r}(0)-\sigma'^1_{\alpha\alpha\,r}(0)\sigma^0_{\alpha\alpha\,i}(0)}{\left|\sigma^0_{\alpha\alpha}(0)\right|^2}t\right]\exp(-\mathrm{j}2\pi f_{\mathrm{D}}t)\mathrm{d}t \\ &= \sigma^0_{\alpha\alpha}(0)\delta\left(2\pi f_{\mathrm{D}}-\frac{\sigma'^1_{\alpha\alpha\,i}(0)\sigma^0_{\alpha\alpha\,r}(0)-\sigma'^1_{\alpha\alpha\,r}(0)\sigma^0_{\alpha\alpha\,i}(0)}{\left|\sigma^0_{\alpha\alpha}(0)\right|^2}\right), \qquad (30)\end{aligned}$$

where $\delta(\bullet)$ denotes the Dirac-delta function.

From Eq. (30), the Doppler shift f_{D} is obtained as

$$f_{\mathrm{D}} = \frac{1}{2\pi}\frac{\sigma'^1_{\alpha\alpha\,i}(0)\sigma^0_{\alpha\alpha\,r}(0)-\sigma'^1_{\alpha\alpha\,r}(0)\sigma^0_{\alpha\alpha\,i}(0)}{\left|\sigma^0_{\alpha\alpha}(0)\right|^2}. \tag{31}$$

5. Numerical results

The sea surface spectra at a given time for various wind speeds are compared in Fig. 1. Here $t = 0$ s. As shown in Fig. 1, it is obvious that for large spatial wave numbers the spectrum for the Barrick model has orders of magnitude larger than the spectra for the other two models. This is because, for large values of the spectral parameter K, Eq. (17) has two regions of the q-integral which gives a leading-order contribution, small q and small $K - q$. From Fig. 1, we can also note that the spectrum corresponding to the Creamer model agrees with the spectrum for the linear hydrodynamic model.

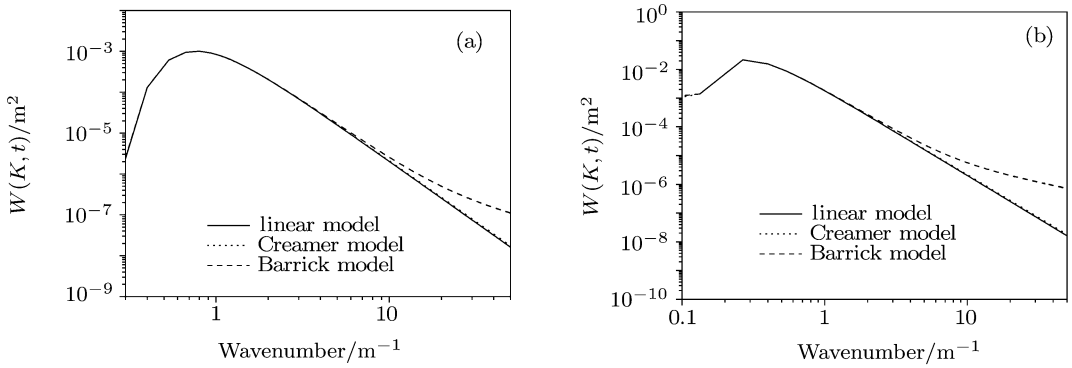


Fig. 1. Sea surface spectrum $W(K,t)$ versus spatial wave number for different wind speeds: (a) $U = 3$ m/s; (b) $U = 5$ m/s.

The comparisons of the dispersion relationships for different sea surface models are shown in Fig. 2. Here $t = 0$ s. From Fig. 2, one can find that the anglular frequencies corresponding to the Creamer sea surface are larger than those for the Barrick and the linear hydrodynamic models. The anglular frequencies for the Barrick sea surface are inconsistent with the results obtained by the linear surface model. Comparing Fig. 2(a) with Fig. 2(b), we can also find that the results for the Barrick and the linear hydrodynamic models are insensitive to the wind speeds. On the other hand, the anglular frequencies for the Creamer surface waves increase with wind speed.

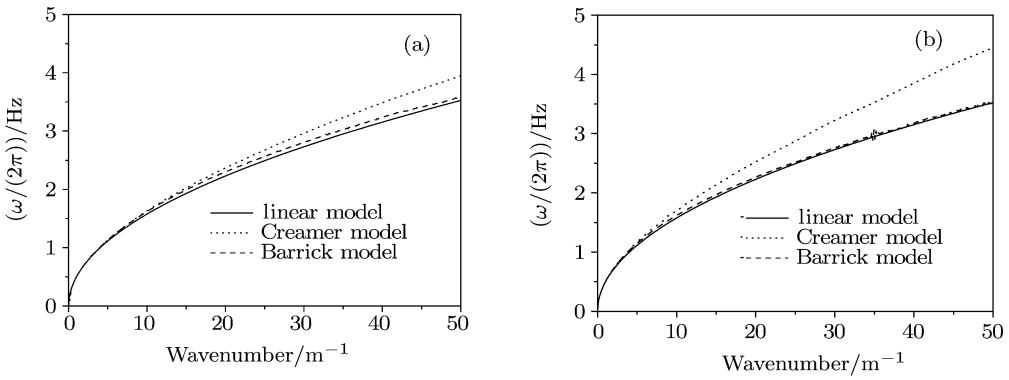


Fig. 2. Dispersion relationship diagrams for different wind speeds: (a) $U = 3$ m/s, (b) $U = 5$ m/s.

In Fig. 3, the backscattered NRCS for the three hydrodynamic models are illustrated at 3 m/s wind speed. Here the radar frequency equals 1.3 GHz (L-band). From Fig. 3, it is noted that the scattered results from the Barrick surface are larger than those from linear and Creamer surfaces for both HH and VV polarisations. It can be explained by the Bragg-scattering mechanism. For Bragg scattering the NRCS is in proportion to the sea surface spectrum, i.e. $\sigma_{\mathrm{B}} \propto W(2k \sin\theta_{\mathrm{i}})$. Therefore, for large spatial wave numbers $(2k \sin\theta_{\mathrm{i}})$ the magnitude of the sea spectrum for the Barrick model is larger than that of the other two sea spectra. From Fig. 3, we also find that the NRCS from the Creamer sea surface is inconsistent with the results from the linear model due to the agreement between the spectra of the Creamer and the linear sea surface.

In Fig. 4, we present the Doppler shift as a function of the incident angle for three radar frequencies, 1.0 GHz, 1.3 GHz and 1.5 GHz. Here the wind speed is 3 m/s. As shown in Fig. 4, the Doppler shifts become larger with the increase of the radar frequency. And we can also find that the Doppler shifts for the Creamer model are some what larger than the results for the linear and the Barrick models. The main reason is that the anglular frequency for the Creamer sea wave is larger than those corresponding to the Barrick and the linear sea waves.

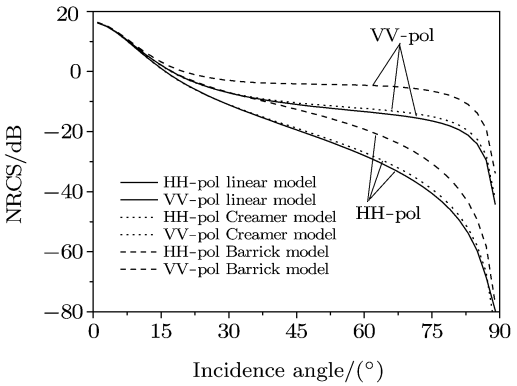


Fig. 3. Backscattering NRCS versus incident angle for different hydrodynamic models.

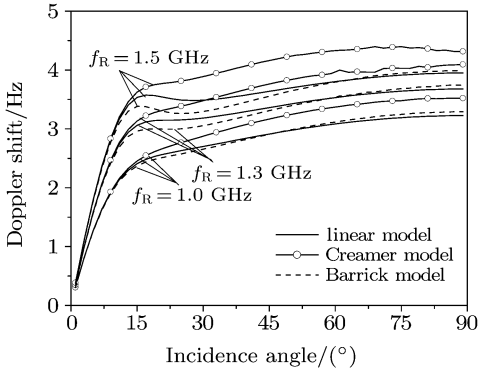


Fig. 4. Doppler shifts versus incident angle for different radar frequencies.

In Fig. 5, the Doppler shifts as a function of the incident angle for various wind speeds are presented. Here, the radar frequency is equal to 1.3 GHz (L-band). For comparisons, we also indicate on both figures the Doppler shifts associated to the resonant Bragg waves and the so-called long waves in the framework of the geometrical optics method. The Bragg shifts $f_B(\theta_i)$ can be evaluated by[21]

$$f_B(\theta_i) = \frac{1}{2\pi}\sqrt{gK_B} \tag{32}$$

with $K_B = 2k\sin(\theta_i)$.

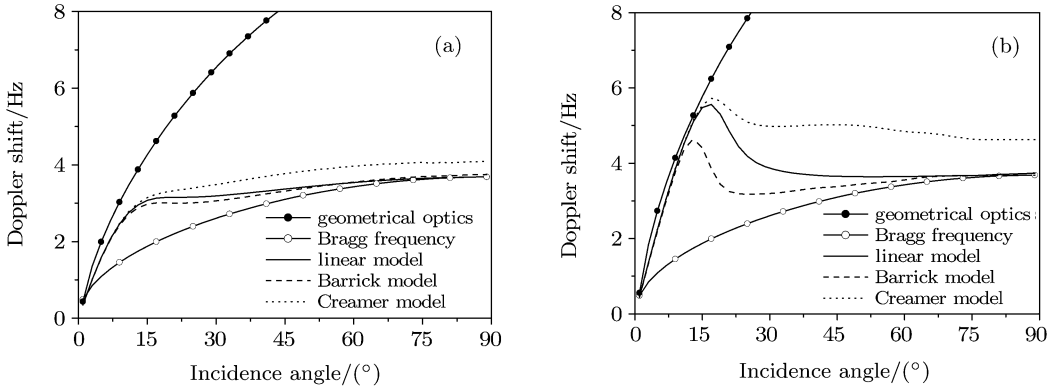


Fig. 5. Doppler shifts versus incident angle for different wind speeds: (a) $U = 3$ m/s, (b) $U = 5$ m/s.

For geometrical optics approximation, the Doppler shifts $f_O(\theta_i)$ induced by the so-called long waves and the mean phase speed $\bar{v}$ in the line-of-sight of the radar are related by the following relation

$$f_O(\theta_i) = \frac{k\sin(\theta_i)}{\pi}\bar{v}, \tag{33}$$

where the detected mean phase speed is[22]

$$\bar{v} = \frac{\int_0^{K_B/3} v(\kappa)\kappa^2 W(\kappa)\mathrm{d}\kappa}{\int_0^{K_B/3} \kappa^2 W(\kappa)\mathrm{d}\kappa}. \quad (34)$$

The Doppler shifts induced by the Bragg waves and the so-called long waves indicated the asymptotic limits of the solution. From Fig. 5, it is obvious that the results given by SSA-I for the linear and the Barrick hydrodynamic models lead to predictions between these two limits. The smaller is the incident angle, the closer to the geometrical optics solution are the simulations. As the incident angle increases, the Doppler shifts for the linear and the Barrick hydrodynamic models tend toward the Bragg results. However, we observe that at large incident angles the Doppler shifts corresponding to the Creamer model are larger than the Bragg results. Comparing Fig. 5(a) with Fig. 5(b), it is found that at small to moderate incident angles the Doppler shifts for these three hydrodynamic models increase with the wind speed. However, at larger incident angles the results corresponding to the linear and the Barrick models are insensitive to the wind speed and this phenomenon is not coincident with the measured data.[23,24]

6. Conclusions

In this paper, time dependent asymptotic solutions have been derived to predict Doppler shifts by using SSA-I for three different hydrodynamic sea surface models: a linear model, the nonlinear Barrick model and the nonlinear Creamer model. As shown, for large spatial wave numbers the sea surface spectrum for the Barrick model is larger than the spectra corresponding to the other two models. On the other hand, for the harmonic wave with the same wave number the angular frequency for the Creamer model is larger than those corresponding to the Barrick and the linear sea surfaces. The Doppler shifts predicted by SSA-I for these three sea surface models are all dependent on radar frequency, wind speed and incident angle. With the increase of the radar frequency, the Doppler shifts became larger. At small and moderate incident angles, the Doppler shifts for the three models increase with wind speed. Nevertheless, at larger incident angles, the results for the linear and the Barrick models are insensitive to the wind speed and this is not coincident with the experimental data.

Although this paper is limited to 1-D sea surface, the conclusions obtained in this paper are helpful to better understand the sensitivity of radar signals to both the sea surface characteristics and the radar parameters.

References

[1] McGregor J A, Poulter E M and Smith M J 1997 *J. Geophys. Res.* **102** 25227
[2] Johannessen J A 2008 *J. Geophys. Res. Lett.* **35** 1
[3] Soriano G, Joelson M and Saillard M 2006 *IEEE Trans. Geosci. Remote Senging* **44** 2430
[4] Guo L X, Wang R, Wang Y H and Wu Z S 2008 *Acta Phys. Sin.* **57** 3464 (in Chinese)
[5] Guo L X, Wang Y H and Wu Z S 2005 *Acta Phys. Sin.* **54** 96 (in Chinese)
[6] Zhang Y M, Wang Y H and Guo L X 2010 *Chin. Phys.* B **19** 054103
[7] Zavorotny V U and Voronovich A G 1998 *IEEE Trans. Antennas Propagat.* **46** 84
[8] Romeiser R and Thompson D R 2000 *IEEE Trans. Geosci. Remote Senging* **38** 446
[9] Mouche A A, Chapron B, Reul N and Collard F 2008 *Waves in Random and Complex Media* **18** 185
[10] Barrick D E 1977 *Remote Sensing of Environment* **6** 201
[11] Barrick D E 1977 *Radio Sci.* **12** 415
[12] Lipa B J 1978 *J. Geophys. Res.* **83** 959
[13] Barrick D E and Weber B L 1977 *J. Phys. Oceanogr.* **7** 11
[14] Creamer D B, Henyey F, Schult R and Wright J 1989 *J. Fluid Mech.* **205** 135
[15] Voronovich A G and Zavorotny V U 2001 *Waves in Random Media* **11** 247
[16] Longuet-Higgins M S 1963 *J. Fluid Mech.* **17** 459
[17] Chen K S, Fung A K and Weissman D E 1992 *IEEE Trans. Geosci. Remote Sensing* **30** 811
[18] Hisaki Y and Tokuda M 1995 *J. Oceanogr.* **51** 385
[19] Johnson J T, Toporkov J V and Brown G S 2001 *IEEE Trans. Geosci. Remote Sensing* **39** 2411
[20] Weber B L and Barrick D E 1977 *J. Phys. Oceanogr.* **7** 3
[21] Toporkov J V and Brown G S 2000 *IEEE Trans. Geosci. Remote Sensing* **38** 1616
[22] Chapron B, Collard F and Ardhuin F 2005 *J. Geophys. Res.* **110** C07008
[23] Trizna D B 1985 *IEEE Trans. Oceanic Eng.* **10** 368
[24] Rozenberg A D, Quigley D C and Melville W K 1996 *IEEE Trans. Geosci. Remote Sensing* **34** 1331